American Journal of Mechanical Engineering, 2015, Vol. 3, No. 3A, 9-14
Available online at http://pubs.sciepub.com/ajme/3/3A/2

DOI:10.12691/ajme-3-3A-2

Computer Simulation of the Aerodynamic Structure of an Arched Roof Obstacle and Validation with Anterior Results

Slah Driss, Zied Driss*, Imen Kallel Kammoun

Laboratory of Electro-Mechanic Systems (LASEM), National School of Engineers of Sfax (ENIS), University of Sfax (US), B.P. 1173, Road Soukra km 3.5, 3038 Sfax, TUNISIA
*Corresponding author: Zied.Driss@enis.rnu.tn

Received May 20, 2015; Revised June 22, 2015; Accepted July 13, 2015

Abstract The present paper is dedicated to the numerical simulation of the aerodynamic structure of an arched roof obstacle with a height h=63 mm and a length L_2=118 mm. The governing equations of mass and momentum in conjunction with the standard k-ε turbulence model are solved using the software "Solid Works Flow Simulation". A finite volume discretization is used. The numerical results are validated with anterior results developed in a wind tunnel. The numerical simulations agreed reasonably with the experimental results and the numerical model was validated.

Keywords: *CFD, turbulent flow, aerodynamic structure, arched roof*

Cite This Article: Slah Driss, Zied Driss, and Imen Kallel Kammoun, "Computer Simulation of the Aerodynamic Structure of an Arched Roof Obstacle and Validation with Anterior Results." *American Journal of Mechanical Engineering*, vol. 3, no. 3A (2015): 9-14. doi: 10.12691/ajme-3-3A-2.

1. Introduction

Green buildings differ from conventional buildings due to the integration social and economic objectives. Environmental considerations roughly correspond direct and indirect environmental impacts, such as reduced emissions of greenhouse gases or reduced water consumption. Social considerations can be directly related to building itself like clean air and comfortable, natural light or beyond the framework Building. In this context, the study of geometry parameters effects on airflow patterns around numerous structures can be done inside wind tunnels, where airflow conditions are controlled. For example, Ntinas et al. [1] conducted an experiment inside a wind tunnel and the air velocity and turbulent kinetic energy profiles were measured around two small-scale obstacles with an arched-type and a pitched-type roof. Luo et al. [2] studied models of cuboid obstacles to characterize the three-dimensional responses of airflow behind obstacles with different shape ratios to variations in the incident flow in a wind-tunnel simulation. Tominaga and Stathopoulos [3] reviewed current modeling techniques in CFD simulation of near-field pollutant dispersion in urban environments and discussed the findings to give insight into future applications. Jiang et al. studied [4] three ventilation cases, single-sided ventilation with an opening in windward wall, single-sided ventilation with an opening in leeward wall, and cross ventilation. In the wind tunnel, a laser Doppler anemometry was used to provide accurate and detailed velocity data. Ahmad et al. [5] provided a comprehensive literature on wind tunnel simulation studies in urban street canyons/intersections including the effects of building configurations, canyon geometries, traffic induced turbulence and variable approaching wind directions on flow fields and exhaust dispersion. Smolarkiewicz et al. [6] performed large-eddy simulations (LES) of the flow past a scale model of a complex building. Calculations are accomplished using two different methods to represent the edifice. De Paepe et al. [7] simulated five different wind incidence angles using a turntable, in order to quantify their effect on indoor air velocities. The responses in local air velocities could largely be attributed to the relative position of the end walls of the scale models orientated towards the wind. This crucial position allows the measured air velocity trends to be explained. Lim et al. [8] presented a numerical simulation of flow around a surface mounted cube placed in a turbulent boundary layer. The simulations were carried at a Reynolds number, based on the velocity at the cube height, of 20,000 large enough that many aspects of the flow are effectively Reynolds number independent. Becker et al. [9] studied the structure of the flow field around three-dimensional obstacles of different aspect ratios, in two different types of boundary layers. The dimensions of the rectangular block obstacles were chosen to represent generic shapes of buildings. De Melo et al. [10] developed two Gaussian atmospheric dispersion models, AERMOD and CALPUFF. Both incorporating the PRIME algorithm for plume rise and building downwash, are inter-compared and validated using wind tunnel data on odour dispersion around a complex pig farm facility comprising of two attached buildings.

Richards et al. [11] used as input data for generating typical weather data required as input for building and heating, ventilation and air-conditioning (HVAC) system models in order to study the energy budgets of buildings and assess the performance of air-conditioning (A/C) systems. Gousseau et al. [12] used Large-Eddy Simulation (LES) to investigate the turbulent mass transport mechanism in the case of gas dispersion around an isolated cubical building. Close agreement is found between wind-tunnel measurements and the computed average and standard deviation of concentration in the wake of the building. Meslem et al. [13] observed changes in the prediction of local and global mean-flow quantities as a function of the considered turbulence model and by the lack of consensus in the literature on their performance to predict jet flows with significant three-dimensionality. The study reveals that none of the turbulence models is able to predict well all the jet characteristics in the same time. Cadirci et al. [14] studied the flow fields generated by a Java in a water channel. Detailed quantitative information about the performance of the Java on a flat-plate boundary layer is obtained. Java-induced boundary-layer profiles are clearly fuller at the wall and hence more resistant to flow separation. The 'positive' effects of the Java with different operating regimes on various boundary-layer flow characteristics such as displacement thickness, shape factor and the friction coefficient are presented. Kassiotis et al. [15] discussed a way to compute the impact of free-surface flow on nonlinear structures. The approach chosen relies on a partitioned strategy to solve the strongly coupled fluid-structure interaction problem. It is then possible to re-use the existing and validated strategy for each sub-problem. The structure is formulated in a Lagrangian way and solved by the finite element method. The free-surface flow approach considers a Volume-Of-Fluid (VOF) strategy formulated in an Arbitrary Lagrangian-Eulerian (ALE) framework, and the finite volume is used to discrete and solve this problem. In this paper, we are interested on the study of the aerodynamic structure of an arched-type roof obstacle placed in a wind tunnel.

2. Numerical Model

The vast majority of fluid flows encountered in aerodynamics are turbulent. The equations governing the air flow called the Navier-Stokes equations are obtained from the continuity equation, the equation of momentum, the transport equation of turbulent kinetic energy k and the transport equation of dissipation rate of turbulent kinetic energy ε. Several methods are available for including turbulence in the Navier-Stokes equations. Most of these involve a process of time-averaging of the conservation equations. When turbulence is included, the transported quantity is assumed to be the sum of equilibrium and a fluctuating component. The only term that remains positive definite is one containing the product of two fluctuating terms [16-23].

2.1. Computational Domain

The considered computational domain is shown in Figure 1. It is defined by the interior volume of the wind tunnel blocked by two planes: the first one is in the entry and the second one is in the exit. The obstacle consists on an arched type roof with a height h=63mm and a width L_2=118 mm. The distance between the obstacle and the entry plane and that between the obstacle and the exits plane are defined by L_1=151 mm and L_3=529 mm respectively.

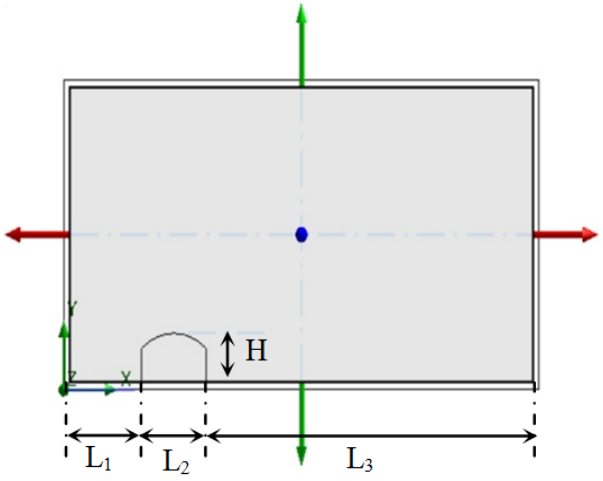

Figure 1. Computational domain for different highs

2.2. Boundary Conditions

The boundary conditions are required anywhere fluid enters or exits the system and can be set as a pressure, mass flow, volume flow or velocity. For the inlet velocity, we will take as a value U_{ref}=0.32 m.s^{-1}, and for the outlet pressure a value of 101325 Pa will be considered which means that at this opening the fluid exits the model to an area of static atmospheric pressure. A summary of the boundary conditions is given in the Figure 2.

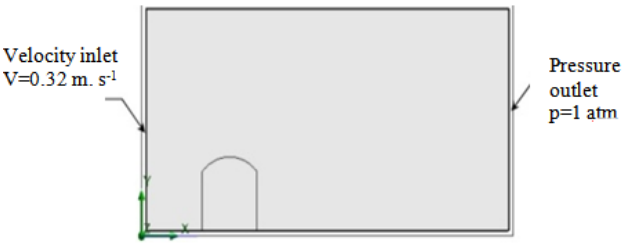

Figure 2. Boundary conditions in the test section

2.3. Mesh Resolution

In several ways, we can control the basic mesh by changing the number of the basic mesh cells along the X, Y and Z axes. The considered geometry can be resolved reasonably well. However, if we generate the mesh and zoom in the roof obstacle, we will see that it may still unresolve. In order to resolve these regions properly, we have used the Local Initial Mesh option (Figure 3). It allows us to specify an initial mesh in a local region of the computational domain to better resolve the model geometry and/or flow particularity in this region. The local region can be defined by a component of the assembly, specified by selecting the model face. All refinement levels are set with respect to the basic mesh cell [16,17,18].

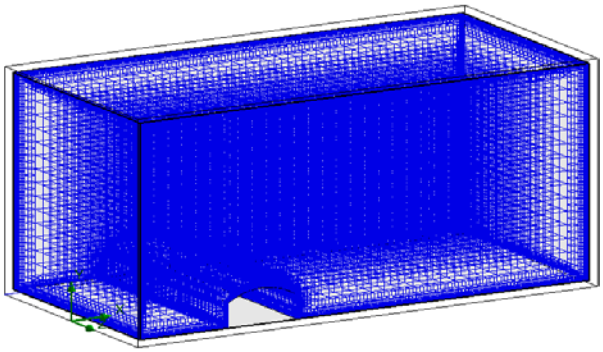

Figure 3. Representation of the basic mesh

3. Numerical Results

3.1. Velocity Field

Figure 4 presents the distribution of the velocity field in the longitudinal and the transverse planes defined by Z=0 mm and X=179 mm. According to these results, it has been noted that the velocity is weak in the inlet of the entry. It is indeed governed by the boundary condition value of the inlet velocity which is equal to 0.32 m.s^{-1}. In this region, the velocity field is found to be uniform and increases progressively downstream of the entry. While the position of the obstacle is characterized by the high velocity. Downstream of the arched type obstacle the velocity keeps increasing progress. Then, a decrease has been noted through the exit where the minimum velocity values are recorded in the lateral walls. The maximum velocity values are located in the top of the roof according to the distribution shown in the Z=0 mm plane. However, in the obstacle downstream a dead zone has been observed in the transverse plane shows a symmetric distribution.

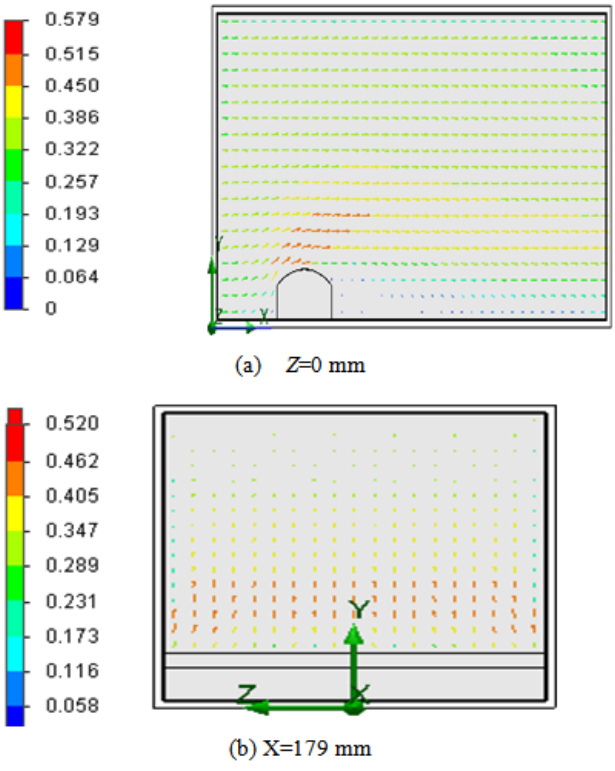

Figure 4. Distribution of the velocity field

3.2. Total Pressure

Figure 5 presents the distribution of the total pressure in the longitudinal and the transverse planes defined by Z=0 mm and X=179 mm. According to these results, it has been noted that a compression zone appears in the obstacle upstream of the obstacle. However, a depression zone has been observed in the downstream of the obstacle. In the top of the test section, the total pressure keeps a uniform distribution. The compression zones are located in the top of the roof. Downstream of the arched type obstacle, the total pressure keeps increasing progress.

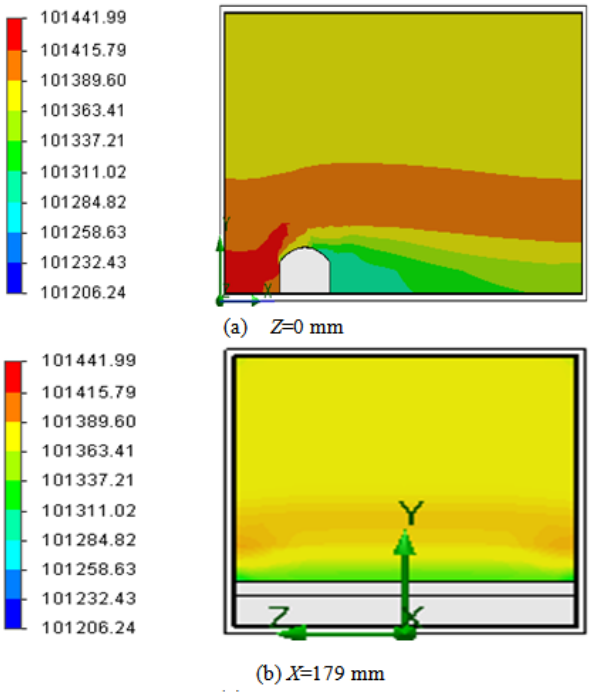

Figure 5. Distribution of the total pressure

3.3. Dynamic Pressure

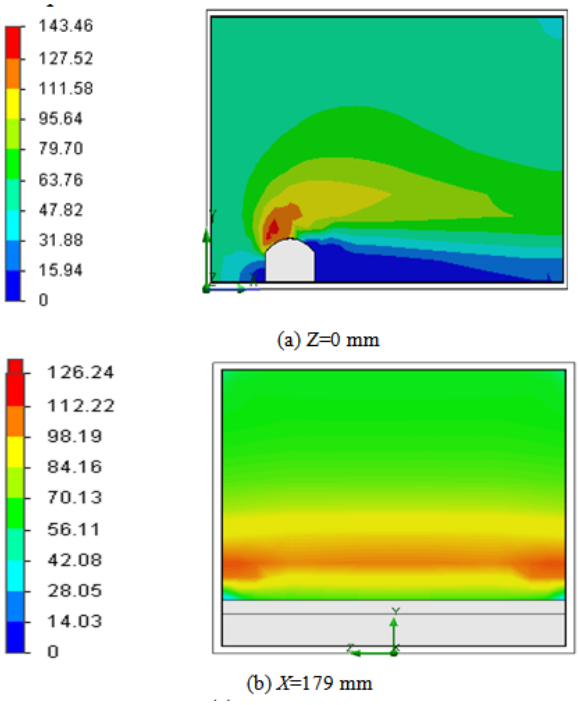

Figure 6. Distribution of the dynamic pressure

Figure 6 presents the distribution of the dynamic pressure in the longitudinal and the transverse planes defined by Z=0 mm and X=179 mm. According to these results, it has been noted that a compression zone appears in the obstacle upstream of the obstacle. However, a depression zone is located in the downstream of the obstacle. In the top of the test section, the dynamic pressure keeps a uniform distribution. Downstream of the arched type obstacle the pressure keeps increasing progress. The maximum pressure values are located in the top of the roof.

3.4. Turbulent Kinetic Energy

Figure 7 presents the distribution of the turbulent kinetic energy in the longitudinal and the transverse planes defined by Z=0 mm and X=179 mm. According to these results, it has been noted that the turbulent kinetic energy is weak in the section inlet. In this region, the turbulent kinetic energy is found to be uniform and increases progressively downstream of the test section. Downstream of the arched type obstacle, the turbulent kinetic energy keeps increasing progress. Then, a decrease has been noted through the exit where the minimum energy values are recorded in the lateral walls. The maximum turbulent kinetic energy values are located in the top of the roof. However, in the obstacle downstream a wake zone characteristic of the minimum values of the turbulent kinetic energy has been observed.

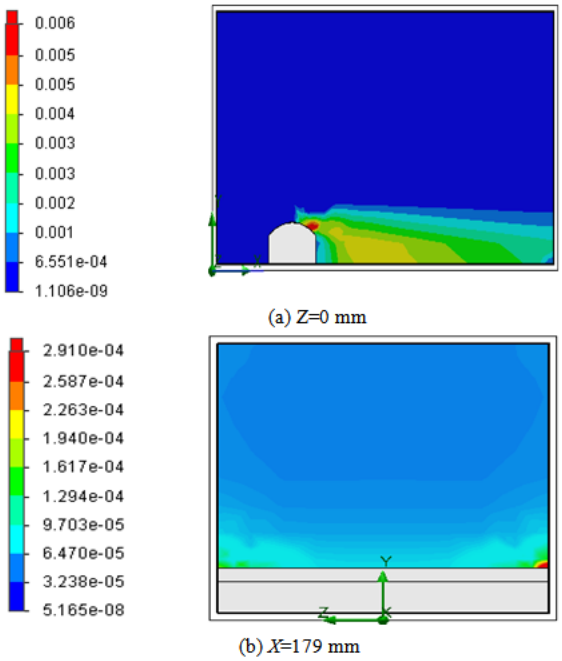

Figure 7. Distribution of the turbulent kinetic energy

3.5. Dissipation Rate of the Turbulent Kinetic Energy

Figure 8 presents the distribution of the turbulent dissipation rate of the turbulent kinetic energy in the longitudinal and the transverse planes defined by Z=0 mm and X=179 mm. From these results, it is clear that the dissipation rate of the turbulent kinetic energy is weak in the inlet of the test section. In this region, the dissipation rate of the turbulent kinetic energy found to be uniform and increases progressively in the test section. Downstream of the arched type obstacle, the dissipation rate of the turbulent kinetic energy keeps increasing progress. Then, a decrease has been noted through the exit where the minimum values of the dissipation rate of the turbulent kinetic energy values are recorded in the lateral walls. The maximum values of the dissipation rate of the turbulent kinetic energy are located in the top of the roof. However, in the obstacle downstream a wake zone characteristic of the minimum value of the turbulent dissipation ratio has been observed.

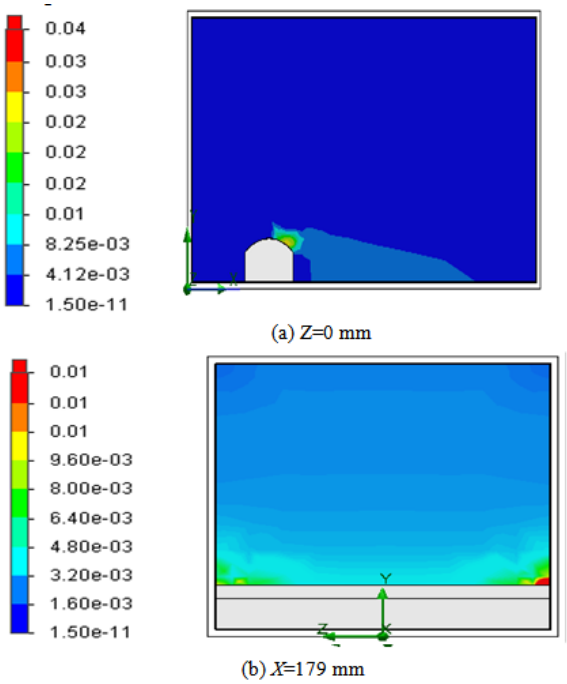

Figure 8. Distribution of the turbulent dissipation rate

3.6. Vorticity

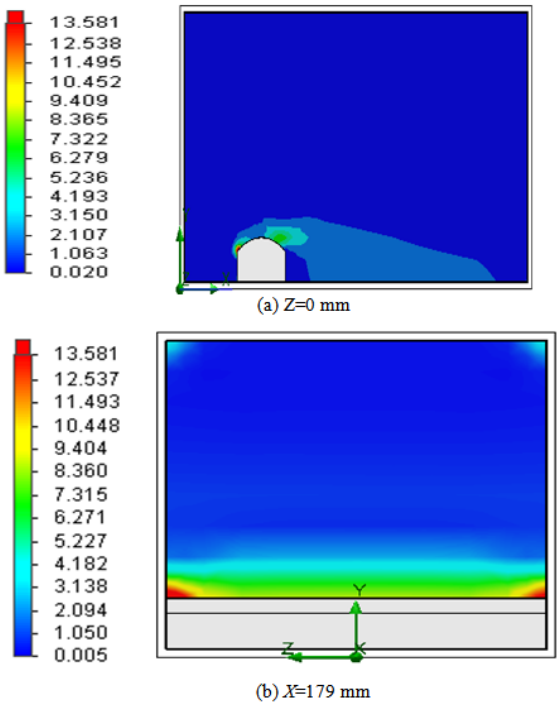

Figure 9. Distribution of the vorticity

Figure 9 presents the distribution of the vorticity in the longitudinal and the transverse planes defined by Z=0 mm and X=179 mm. From these results, it has been noted that the vorticity is weak in the inlet of the test section. In this region, the vorticity is found uniform and increases progressively in the test section. Downstream of the arched type obstacle, the vorticity keeps increasing progress. Then, a decrease has been noted through the exit where the minimum vorticity values are recorded in the lateral walls. The wake characteristic of the maximum vorticity values are located in the top of the roof according. However, in the obstacle downstream the vorticity values vanish.

4. Experimental Validation

The velocity profile around the arched obstacle is presented in Figure 10 for a height h=63 mm and a length L_2=118 mm. These results were predicted along the centre section of the obstacle defined by the plane Z=0 mm and the downstream edges defined by X=6.88 H. The average velocity values were deduced, at each point of the computational domain, by processing the computed values. According to these results, it's clear that the obstacle height has a direct effect on the velocity profile. In fact, the maximum value of the velocity field increases with the increase of the obstacle height. In these conditions, the maximum value of the velocity is equal to V=2.2 Uref. The predicted averaged velocity results are also compared with the measured data of Ntinas et al. [1]. Our numerical results present a good agreement with the experimental data founded from the literature. The gap between results is about 6%. These results confirm the validity of the numerical method.

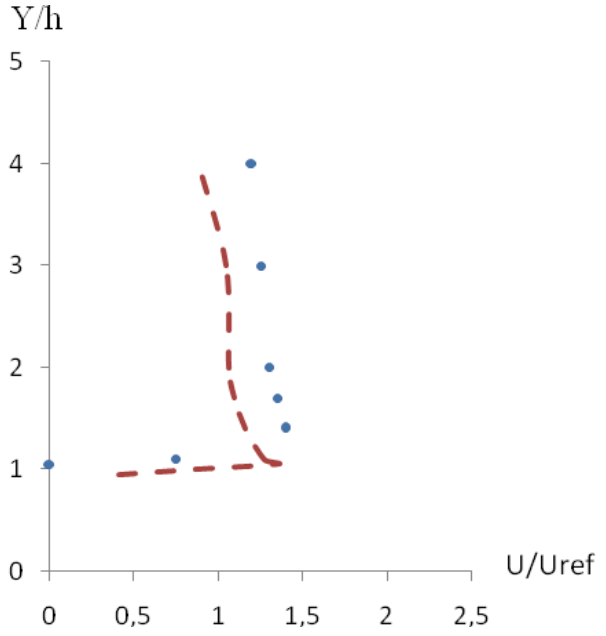

Figure 10. Velocity profile

5. Conclusion

A numerical simulation model was developed to study the aerodynamic structure of arched roof obstacle with a height h=63 mm and a length L_2=118 mm. Numerical results, such as velocity fields, pressure and turbulent characteristics are presented in the considered control volume. The satisfactory agreement between the numerical simulation and the experimental data, from a wind tunnel by anterior results, validated the mathematical model used in this study. According to the obtained results, the velocity keeps increasing progress downstream of the arched type obstacle. Indeed, a decrease has been noted through the exit where the minimum velocity values are recorded in the lateral walls. All these observations are useful for the building design. Particularly, we propose to use this knowledge to optimize ecological buildings.

Nomenclature

H	obstacle height, m
k	turbulent kinetic energy, $J.kg^{-1}$
l	length, m
P	pressure, Pa
Re	Reynolds number
V	magnitude velocity, $m.s^{-1}$
Xi	Cartesian coordinate, m
X	Cartesian coordinate, m
Y	Cartesian coordinate, m
Z	Cartesian coordinate, m
ε	dissipation rate of the turbulent kinetic energy, $W.kg^{-1}$
μ	dynamic viscosity, Pa.s
μ_t	turbulent viscosity, Pa.s
ρ	density, $kg.m^{-3}$

References

[1] G.K. Ntinas, G. Zhang, V.P. Fragos, D.D. Bochtis, Ch. Nikita-Martzopoulou, Airflow patterns around obstacles with arched and pitched roofs: Wind tunnel measurements and direct simulation, European Journal of Mechanics B/Fluids 43 (2014) 216-229.

[2] W. Luo, Z. Dong, G. Qian, J. Lu, Wind tunnel simulation of the three-dimensional airflow patterns behind cuboid obstacles at different angles of wind incidence, and their significance for the formation of sand shadows, Geomorphology 139-140 (2012) 258-270.

[3] Y. Tominaga, T. Stathopoulos, CFD simulation of near-field pollutant dispersion in the urban environment: A review of current modeling techniques, Atmospheric Environment 79 (2013) 716-730.

[4] Y. Jiang, D. Alexander, H. Jenkins, R. Arthur, Q. Chen, Natural ventilation in buildings: measurement in a wind tunnel and numerical simulation with large-eddy simulation, J. Wind Eng. Ind. Aerodyn. 91 (2003) 331-353.

[5] K. Ahmad, M. Khare, K.K. Chaudhry, Wind tunnel simulation studies on dispersion at urban street canyons and intersections- a review, J. Wind Eng. Ind. Aerodyn. 93 (2005) 697-717.

[6] P.K. Smolarkiewicz, R. Sharman, J. Weil, S.G. Perry, D. Heist, G. Bowker, Building resolving large-eddy simulation and comparison with wind tunnel experiments, journal of computational Physics 227 (2007) 633-653.

[7] M. De Paepe, J.G. Pieters, W.M.Cornelis, D. Gabriels, B. Merci, P. Demeyer, Airflow measurements in and around scale-model cattle barns in a wind tunnel: Effect of wind incidence angle, Biosystems Engineering 115 (2013) 211-219.

[8] H.C. lim, T.G. Thomas, Ian P. Castro, Flow around a cube in a turbulent boundary layer: LES and experiment /J. Wind Eng. Ind. Aerodyn. 97 (2009) 96-109.

[9] S. Becker, H. Lienhart, F. Durst, Flow around three-dimensional obstacles in boundary layers, J. Wind Eng. Ind. Aerodyn. 90 (2002) 265-279.

[10] A.M.V. De Melo, J.M. Santos, I. Mavrroidis, N. Costa Reis Junior, Modelling of odour dispersion around a pig farm building complex using AERMOD and CALPUFF. Comparison with wind tunnel results, A.M. Vieira de Melo et al. / Building and Environment 56 (2012) 8-20.

[11] K. Richards, M. Schatzmann, B. Leitl, Wind tunnel experiments modelling the thermal effects within the vicinity of a single block building with leeward wall heating, J. Wind Eng. Ind. Aerodyn. 94 (2006) 621-636.

[12] P. Gousseau, B. Blocken, G.J.F Heijst, Large-Eddy Simulation of pollutant dispersion around a cubical building: Analysis of the turbulent mass transport mechanism by unsteady concentration and velocity statistics, Environmental Pollution 167 (2012) 47-57.

[13] A. Meslema, F. Bodeb, C. Croitorub, I. Nastaseb, Comparison of turbulence models in simulating jet flow from a cross-shaped orifice : European Journal of Mechanics B/Fluids 44 (2014) 100-120.

[14] S. Cadircia, H. Gunesa, U. Ristb, Numerical investigation of a jet and vortex actuator in a cross flow boundary layer: European Journal of Mechanics B/Fluids 44 (2014) 42-59.

[15] C. Kassiotis, A. Ibrahimbegovica, H. Matthiesb, Partitioned solution to fluid–structure interaction problem in application to free-surface flows, European Journal of Mechanics B/Fluids 29 (2010) 510-521.

[16] Z. Driss, M. Ammar, W. Chtourou, MS. Abid, CFD Modelling of Stirred Tanks. Engineering Applications of Computational Fluid Dynamics 5 (2011) 145-258.

[17] Z. Driss, MS. Abid Use of the Navier-Stokes Equations to Study of the Flow Generated by Turbines Impellers. Navier-Stokes Equations: Properties, Description and Applications 3 (2012) 51-138.

[18] S. Driss, Z. Driss, I. Kallel Kammoun, Study of the Reynolds Number Effect on the Aerodynamic Structure around an Obstacle with Inclined Roof, Sustainable Energy, 2014, Vol. 2, No. 4, 126-133.

[19] Z. Driss, MS. Abid, Numerical and experimental study of an open circuit tunnel: aerodynamic characteristics. Science Academy Transactions on Renewable Energy Systems Engineering and Technology 2 (2012) 116-123.

[20] Z. Driss, A. Damak, S. Karray, MS. Abid, Experimental study of the internal recovery effect on the performance of a Savonius wind rotor. Research and Reviews: Journal of Engineering and Technology 1 (2012) 15-21.

[21] Z. Driss, G. Bouzgarrou, W. Chtourou, H. Kchaou, MS. Abid, Computational studies of the pitched blade turbines design effect on the stirred tank flow characteristics, European Journal of Mechanics B/Fluids 29 (2010) 236-245.

[22] M. Ammar, W. Chtourou, Z. Driss, MS. Abid, Numerical investigation of turbulent flow generated in baffled stirred vessels equipped with three different turbines in one and two-stage system, Energy 36 (2011) 5081-5093.

[23] Z. Driss, O. Mlayeh, D. Driss, M. Maaloul, M.S. Abid, Numerical simulation and experimental validation of the turbulent flow around a small incurved Savonius wind rotor, Energy, 74. 506-517, 2014.